ADVANCED FUNCTIONAL MATERIALS
www.afm-journal.de

Cancer-Targeted Monodisperse Mesoporous Silica Nanoparticles as Carrier of Ruthenium Polypyridyl Complexes to Enhance Theranostic Effects

*Lizhen He, Yanyu Huang, Huili Zhu, Guanhua Pang, Wenjie Zheng, Yum-Shing Wong, and Tianfeng Chen**

Mesoporous silica nanoparticles (MSNs) have been well-demonstrated as excellent carriers for anticancer drug delivery. Presented here is a cancer-targeted MSNs drug delivery system that allows the direct fluorescence monitoring of the cellular uptake and localization of theranostic agents in cancer cells. Specifically, the anticancer action mechanisms of RGD peptide-functionalized MSNs carrying ruthenium polypyridyl complexes (RuPOP@MSNs) are elucidated in detail. RGD peptide surface decoration significantly enhances the cellular uptake of the nanoparticles through receptor-mediated endocytosis, and increases the selectivity between cancer and normal cells. RuPOP@MSNs exhibits unprecedented enhanced cytotoxicity toward cancer cells overexpressing integrin receptor, which is significantly higher than that of free RuPOP, through induction of apoptosis. The important contribution of extrinsic pathway to cell apoptosis is confirmed by increase in expression levels of death receptors, activation of caspase-8 and truncation of Bid. The internalized nanoparticles release free RuPOP into the cytoplasm, where they modulate the phosphorylation of p53, AKT, and MAPKs pathways to promote cell apoptosis. Moreover, the strong autofluorescence of RuPOP permits the direct monitoring of drug delivery, and extends the power of theranostics to subcellular level. Taken together, this study provides an effective strategy for the design and development of cancer-targeted theranostic agents.

1. Introduction

Cancer nanotechnology displays potent applications in targeted drug therapy, molecular diagnosis and molecular imaging.[1–4] Nanodrug delivery systems are expected to depress the toxic side effects and simultaneously enhance the therapeutic efficiency, and thus have drawn more and more attention in the past years.[5] Till now, various biocompatible nanosystems with different structure and compositions, such as metals, polymers, oxides, and semiconductors, have been designed and prepared to carry anticancer drugs.[6–8] Among these nanomaterials, mesoporous silica nanoparticles (MSNs) have been well documented as excellent drug delivery and disease-detection systems owing to their straightforward synthesis, tunable pore morphologies, facile functionalization chemistries, high drug loading capability, low-toxicity degradation pathways in the biological milieu, and capacity to carry disparate payloads (molecular drugs, proteins, other nanoparticles) within the porous core.[9–16] The property of easy surface modification/bioconjugation endowed MSNs as an ideal vehicle for targeting imaging, diagnosis, delivery and triggered drug release.[6,13,17–21] Recent studies also supported the use of MSNs as a delivery system for hydrophobic anticancer drugs to overcome their insolubility problem.[22,23] Interestingly, MSNs was found able to enhance the cytotoxicity of anticancer platinum drugs by improving localized drug delivery and facilitating the drug hydrolysis.[24] However, the effects of MSNs on the action mechanisms of the loaded drugs remain elusive.

The limitations of cisplatin-based chemotherapy have kindled great interest of scientists to search alternative metal-based anticancer drugs.[25,26] Ruthenium (Ru) possesses several favorable properties suitable for rational drug design and medicinal applications, such as the high coordination number and low toxicity toward healthy tissues.[27,28] Till now, a great many of Ru complexes have been designed and found to exhibit promising anticancer activities, and two of them, NAMI-A and KP109, have entered clinical trials.[27–30] The rich photophysical properties of Ru complexes render them as excellent DNA structural probes and cellular imaging agents.[31–38] However, the discovery of cancer-selective agents and the clear understanding of the action mechanisms are the critical obstacle and challenge for the clinical development of Ru

L. He, Y. Huang, G. Pang, Prof. W. Zheng, Prof. T. Chen
Department of Chemistry, Jinan University
Guangzhou 510632, China
E-mail: tchentf@jnu.edu.cn
Prof. Y.-S. Wong
School of Life Science and State Key Laboratory for Agrobiotechnology, The Chinese University of Hong Kong
Hong Kong S.A.R, China
Dr. H. Zhu
Medical College, Jinan University
Guangzhou 510632, China

DOI: 10.1002/adfm.201303533

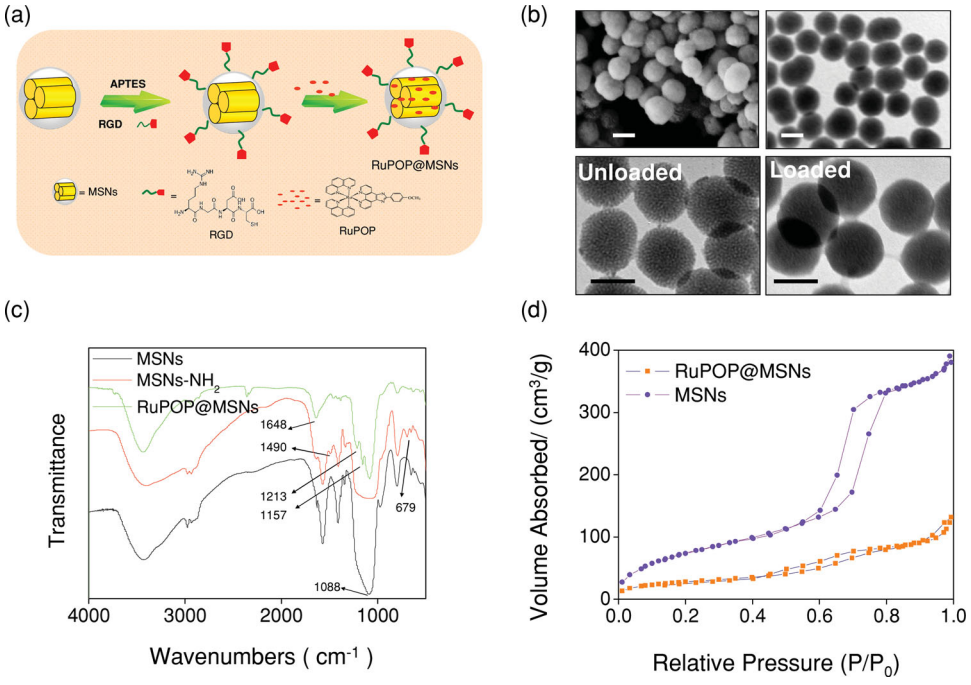

Figure 1. Structural characterization of RuPOP@MSNs. a) Synthetic scheme for the RuPOP@MSNs. b) SEM and TEM images of MSNs. Scale bars is100 nm. c) FT-IR spectra of MSNs, MSNs-NH2, and RuPOP@MSNs. d) N2 adsorption-desorption isotherm for MSNs and RuPOP@MSNs.

complexes. We have previously found that, RuPOP ([Ru(phen)$_2$ p-MOPIP](PF$_6$)$_2$·2H$_2$O), a potent Ru polypyridyl complex with novel anticancer activity higher than cisplatin and strong autofluorescence, could target cancer cell mitochondria and activate intrinsic cell apoptosis.[27] Unfortunately, the further clinical application of RuPOP also was limited by its low aqueous solubility. Therefore, it is of great significance to construct delivery systems for hydrophobic Ru complexes.

MSNs has been widely investigated for their ability to deliver hydrophobic compounds into cancer cells to overcome their insolubility problem.[22–24] Targeting modification could enhance the recognization and internalization of MSNs by cancer cells, thus reduce the administrated dosage and undesirable toxic side effects. To date, various targeting molecules has been conjugated to the surface of MSNs, such as mannose, folic acid, transferrin, TAT, and RGD.[6,23] The RGD (arginine-glycine-aspartic acid) peptide, a particularly effective targeting agent, could be recognized by $\alpha v\beta 3$ integrin receptor overexpressed in various human cancers cells.[39–41] Peptides containing RGD sequence have been identified as ideal targeting molecules for various nanoarchitectures, such as polymers, liposomes, and inorganic nanoparticles, because of its defined structure and small molecular weight. Herein we report a novel cancer-targeted nanodrug delivery system based on RGD peptide-conjugated MSNs loaded with fluorescent Ru complex. This system allows the direct fluorescence monitoring of the cellular uptake and releases of RuPOP in cancer cells, and dramatically enhance the anticancer efficacy of the hydrophobic Ru complex. We also clarified the molecular mechanisms accounting for the action of RuPOP@MSNs.

2. Results and Discussion

2.1. Preparation and Characterization of RuPOP@MSNs

In this study, firstly, MSNs were successfully created by the synthetic route outlined in **Figure 1**a, and characterized by SEM and TEM. As shown in Figure 1b, the SEM and TEM images of the MSNs appear as highly monodisperse particles with a diameter of about 100 nm. As examined by a Zetasizer Nano-ZS particle analyzer, the average particles size of MSNs was about 118.1 nm (Figure S1, Supporting Information). The RGD conjugation and drug loading didn't affect the size and dispersity of MSNs (Figure 1b). FTIR was used to confirm the amination of MSNs and the successful conjugation of RGD to MSNs. As shown in Figure 1c, the peaks at 1490 and 679 cm^{-1} in MSNs-NH$_2$ were assigned to the symmetrical bending vibration of amino groups and the bending vibration of N-H, respectively. The spectrum of MSNs-NH$_2$ retain the special peaks of MSNs. Compared with MSNs, RGD-conjugated MSNs displays two special peaks of amide bands I and II at 1644 and 1554 cm^{-1} (Figure S2, Supporting Information). We also found these peaks of RuPOP@MSNs, such as 1648 cm^{-1} (amide band I from RGD peptide), 1088 cm^{-1} (antisymmetric vibration of Si-O-Si from MSNs), 1213 cm^{-1} (symmetrical stretching vibration of C–O–C from RuPOP) and 1157 cm^{-1} (stretching vibration of C–N from RuPOP).

The presence of RGD peptides was further verified by using a protein staining BCA assay and UV–vis spectroscopy. As shown in Figure S3 (Supporting Information), the UV–Vis spectrum shows an increase in absorbance at 595 nm, due to the presence of protein in the nanoparticles, which was also confirmed by the change in particle color. Moreover, RuPOP@

MSNs exhibits similar emission spectrum with pure RuPOP (Figure S4, Supporting Information), indicating the presence of RuPOP in MSNs. Furthermore, from the results of N_2 adsorption-desorption isotherm (Figure 1d), the inflection point at the adsorption branches of the isotherm of RuPOP@MSNs move to the direction of the low relative pressure, indicating the decline of the quantity of nitrogen capillary condensation. Compared with MSNs, the surface area, pore volume and pore size of RuPOP@MSNs decreased significantly (Table S1, Supporting Information). These results demonstrate the successful loading of RuPOP into the nanoparticles. As shown in **Figure 2**a, the presence of Ru 3p peak at 462.4 eV in the XPS spectrum of RuPOP@MSNs further confirmed the successful loading of RuPOP into MSNs. This increase in the binding energy of N 1s from MSNs-NH_2 suggests the formation of hydrogen bond between RuPOP and the amino groups on the surface of MSNs (Figure 2b). Taken together, these results demonstrate the successful construction of RuPOP@MSNs system.

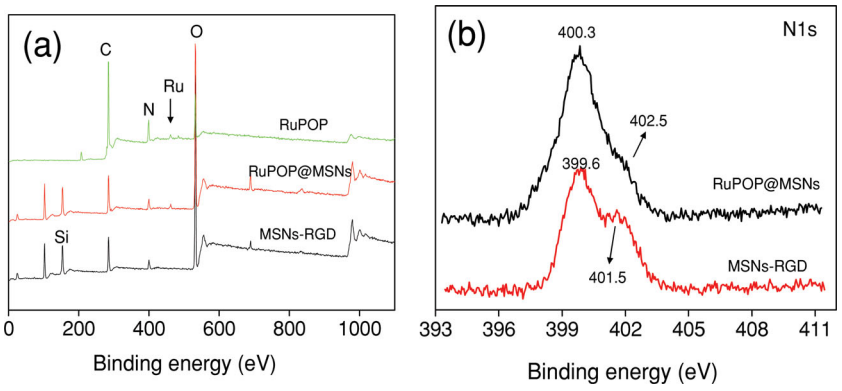

Figure 2. a) XPS spectra of RuPOP, RuPOP@MSNs and MSNs-RGD. b) N 1s spectra of RuPOP@MSNs and MSNs-RGD.

2.2. In Vitro Cellular Uptake of RuPOP@MSNs

Cellular uptake efficacy is an important factor that determines the nanomaterials-based drug activities. Usually, nanomaterials enter cancer cells through passive and active targeting process, and thus could serve as drug carriers of chemotherapeutics. However, passive strategy has limitations due to its random delivery mode.[9] In this study, RGD peptide in the surface of RuPOP@MSNs could recognize and bind to the integrin receptor overexpressed in cancer cell membrane, thus enhance the cellular uptake of the nanoparticles through active targeting process (**Figure 3**a). To examine the contribution of integrin receptor to the cellular uptake of RuPOP@MSNs, firstly, we should examine the expression level of the receptor on the cell membrane. As shown in Figure 3b, the expression levels of

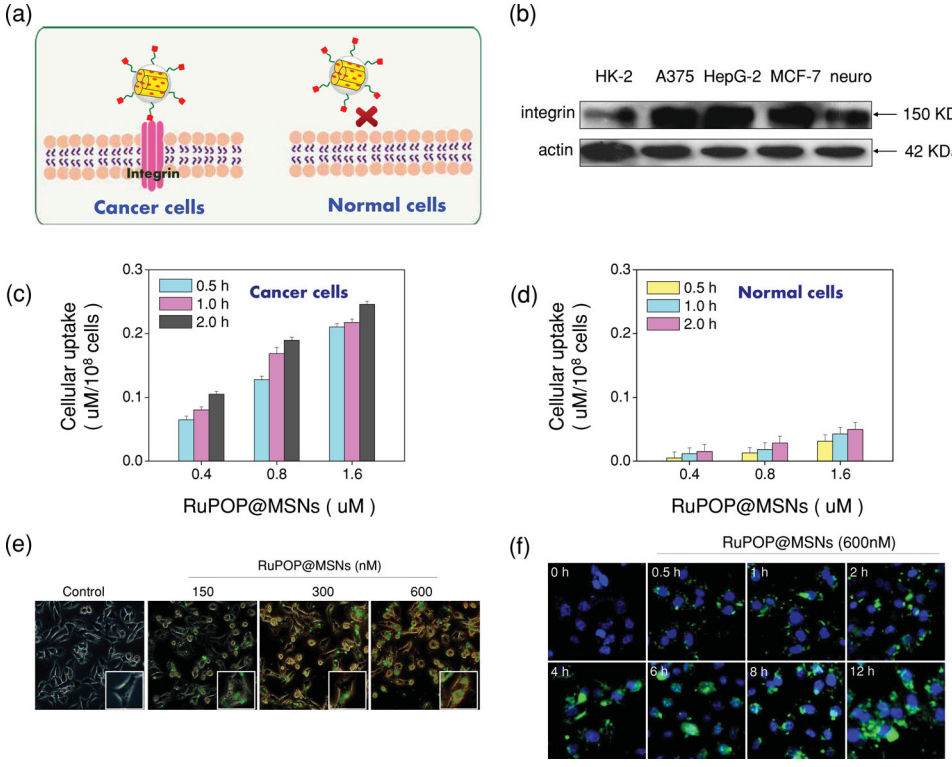

Figure 3. Selective cellular uptake of RuPOP@MSNs. a) Schematic illustration for the targeting effects of RuPOP@MSNs on cancer cells. b) Western blots showing the distinct expression of integrin receptor in various cell lines. c,d) Quantitative analysis of cellular uptake of RuPOP@MSNs in c) A375 and d) HK-2 cells by determination of fluorescence intensity. e) Real-time imaging of the same A375 cells treated with 600 nM RuPOP@MSNs. The RuPOP@MSNs and cell nucleus were visualized by green and blue fluorescence, respectively. f) Quantitative analysis of cellular uptake efficiency of RuPOP@MSNs in A375 cells after treated with the 1.4 mg mL^{-1} of RGD for 1 h.

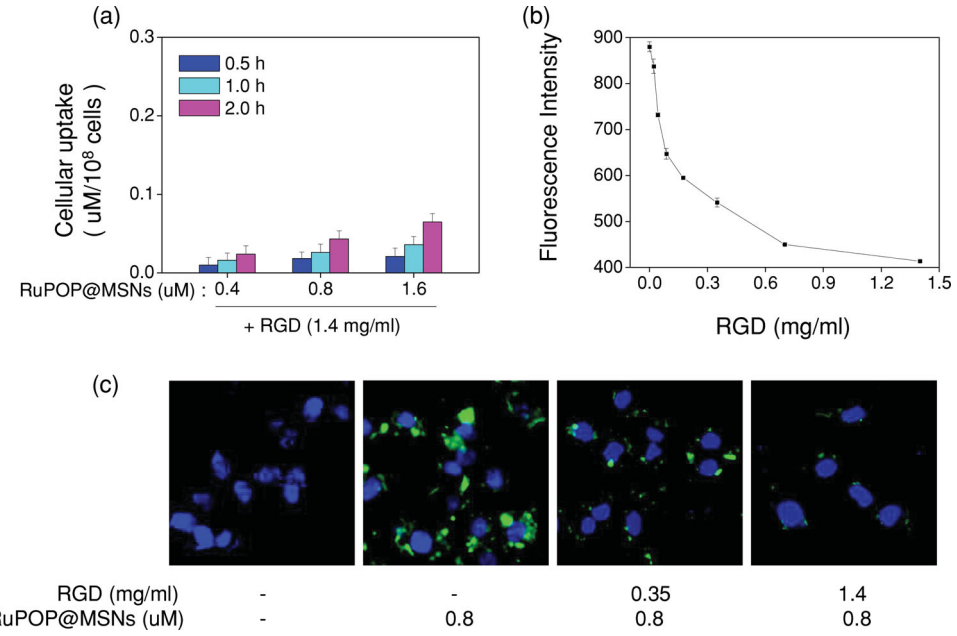

Figure 4. RGD blocks the cellular uptake of RuPOP@MSNs. a) Quantitative analysis of cellular uptake efficiency of RuPOP@MSNs in A375 cells after treated with the 1.4 mg mL^{-1} of RGD for 1 h. (b) Dose-dependent effects of RGD on the cellular uptake of RuPOP@MSNs. The cells were treated with different concentrations of RGD for 1 h, and then exposed to 0.8 μM RuPOP@MSNs for 2 h. cellular uptake was determined by fluorometry as described in Experimental Section. c) Representative fluorescence microscope images showing the internalization of RuPOP@MSNs in A375 cells after 2 h incubation. Cells were pretreated with different concentrations of RGD for 1 h.

integrin receptor in human cancer cells (A375, HepG2, MCF-7, and Neuro-2a) were significantly higher than the HK-2 normal cells. These results suggest the feasibility of the RGD peptide-guided selectivity between cancer and normal cells.

The strong autofluorescence of RuPOP permits the direct monitoring of drug uptake and delivery. Therefore, a quantitative analysis of cellular uptake of nanoparticles in A375 human melanoma cells with high expression level of integrin receptor was conducted by measuring the fluorescence intensity of RuPOP. As shown in Figure 3c, intracellular drug concentration increased in a time- and dose-dependent manner in cancer cells. For instance, after 2-h incubation with 0.4, 0.8, and 1.6 μM of the RuPOP@MSNs, the intracellular RuPOP concentration increased to 0.10, 0.19, and 0.25 μM/10^8 cells, respectively, which were about 5–6 times higher than those in HK-2 human normal cells (Figure 3d). The green fluorescence from the cytoplasm of A375 cells further confirmed the internalization of RuPOP@MSNs (Figure 3e). A detailed time-course analysis showed that RuPOP@MSNs accumulated in the cell membrane after 30 min of treatment and the internalized nanoparticles increased after that in a time-dependent manner (Figure 3f). RGD peptide competing assay was used to further confirm the important role of integrin receptor. As shows in the **Figure 4**a, RGD peptide significantly inhibited the uptake of RuPOP@MSNs in a dose-dependent manner, to the level similar to that in HK-2 human normal cells. Moreover, from the results of fluorescence microscopy, RGD effec tively blocked the internalization of RuPOP@MSNs in A375 cells (Figure 4b,c). These results demonstrate that, the selective uptake of RuPOP@MSNs in human cancer cells could be traced to integrin receptor-mediated endocytosis.

2.3. Endocytosis of RuPOP@MSNs and pH-Mediated Drug Release

Endocytosis is a important uptake mechanism of nanomaterials in cancer cells.[42] In this study, the localization of the RuPOP@MSNs in cancer cells were investigated by using specific probes, Lyso Tracker Red for fluorescence imaging of lysosomes and DAPI (blue) for nucleus. As shown in **Figure 5**a, the complete merge of the green and red fluorescence clearly indicated the colocalization of RuPOP@MSNs and lysosomes, suggesting RuPOP@MSNs entered the cells through endocytosis via lysosomes. In the detailed time-course analysis, we found that RuPOP@MSNs gathered around the cell membrane after 0.5 h of treatment and the fluorescence intensity increased after that. After 4 h of treatment, the nanoparticles entered the lysosomes. From the time point of 12 h, RuPOP was release from lysosomes into the cytosol. Moreover, co-localization of the fluorescence of RuPOP and nucleus was not found, indicating that nucleic acids were not the cellular target of RuPOP@MSNs.

In vitro drug release profiles of RuPOP from the MSNs in PBS at pH 7.4 and 5.3 were investigated to simulate the normal body blood and acidic environments of lysosomes. As shown in Figure 5b, RuPOP was released slowly at first day under two pH conditions, with release ratio at 23.6% for pH 5.3 and 15.3% for pH 7.4, respectively. Thereafter, the cumulative release of RuPOP reached 63.3% for pH 5.3 and 43.1% for pH 7.4 after 12 days. These results demonstrate that the release process at pH 5.3 was much faster than that at pH 7.4. Therefore, MSNs could control the release of RuPOP in acidic microenvironment around the tumor tissues, but not in the normal tissues. Possibly, the faster release of RuPOP under the acidic pH could

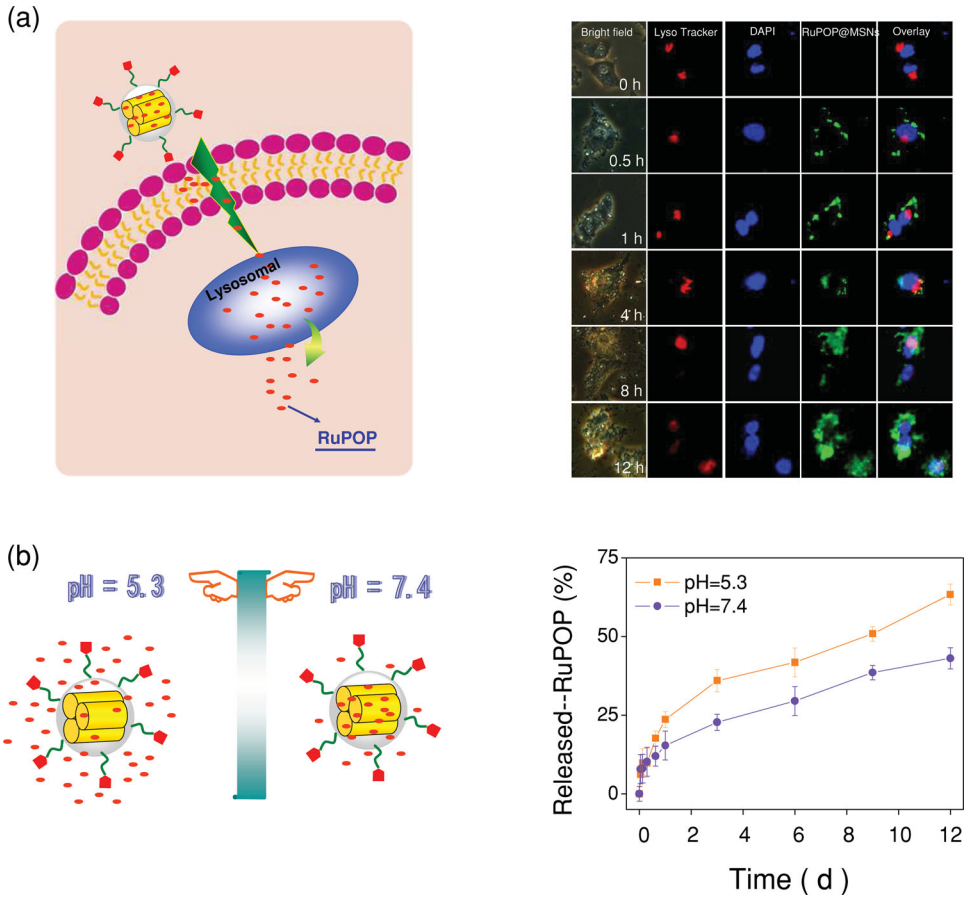

Figure 5. Intracellular localization and release of RuPOP@MSNs. a) Colocalization of RuPOP@MSNs (green fluorescence), nucleus (blue fluorescence), and lysosomes (red fluorescence) in A375 cells. The cells was treated with 600 nM RuPOP@MSNs for different periods of time and visualized under fluorescence microscope. b) In vitro release profiles of RuPOP@MSNs in PBS at different pH values.

be attributed to the interaction mode between RuPOP molecule and the functional groups on the surface of MSNs. Although the successful conjugation of RGD to MSNs, there is plenty of amino groups remained on the surface of the nanomaterials. Therefore, after the loading of RuPOP, hydrogen bond could be formed between RuPOP and the amino groups. This hypothesis could be supported by the increase in the binding energy of N 1s in RuPOP@MSNs by comparing with RGD-MSNs (Figure 2b). However, under the acidic pH condition, protonation of the amino groups would occur, and thus RuPOP was replaced and released into the solution, finally resulted in faster and higher drug release by comparing with that pH 7.4. The results also demonstrated that the RuPOP@MSNs can realize the sustained release and possibly show a longer blood-circulation lifetime in human bodies.

2.4. In Vitro Anticancer Activity of RuPOP@MSNs

This study aimed to use RGD peptide-conjugated MSNs as a carrier of RuPOP to overcome its drawbacks of low aqueous solubility, difficulty in penetrating cell membrane and low selectivity between cancer and normal cells to enhance its anticancer efficacy, therefore, we investigated the effects of RuPOP@MSNs on a series of cancer cells by MTT assay by comparing with RuPOP. As shown in **Figure 6**a, the RuPOP@MSNs exhibited significant anticancer activities against A375 melanoma, HepG2 hepatocellular carcinoma, MCF-7 breast adenocarcinoma, Neuro-2a neuroblastoma and RHepG2 drug-resistant hepatocellular carcinoma cells. The IC_{50} of these cancer cells treated by RuPOP@MSNs was declined about 30–90 times of RuPOP (Figure S5, Supporting Information). Especially, A375 cells displayed the highest sensitivity to RuPOP@MSNs with IC_{50} found at 65.8 nM, while the IC_{50} value for free RuPOP was 5.9 μM. A time-course analysis revealed that RuPOP@MSNs exhibited time- and dose-growth inhibition on A375 and MCF-7 cells. Significant growth inhibition was also observed in cells treated with RuPOP@MSNs for 24 h (Figure S6, Supporting Information). In contrast, the nanodrug carrier RGD-MSNs alone showed no cytotoxicity toward various cancer and normal cells, even at concentrations of 200 and 400 μg mL^{-1} (Figure S7, Supporting Information). Furthermore, the toxicity of RuPOP@MSNs toward HK-2 human normal cells was much lower than that of RuPOP (Figure 6b). These results indicate that RuPOP@MSNs exhibits higher anticancer efficacy and lower toxicity than RuPOP.

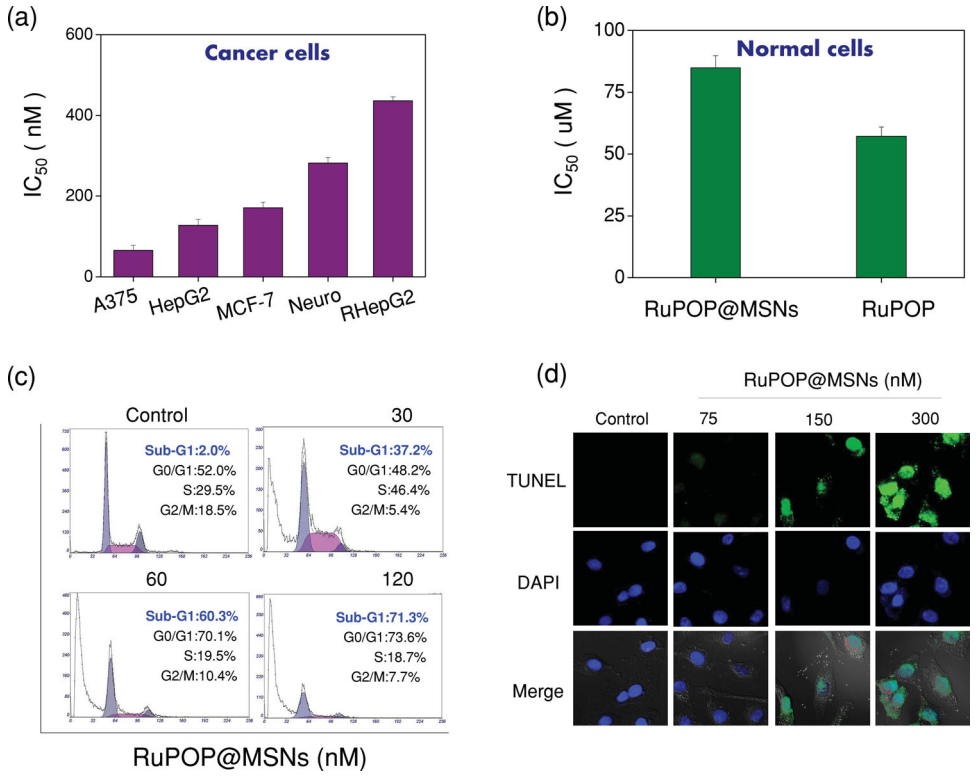

Figure 6. Induction of apoptosis in cancer cells after by RuPOP@MSNs. a,b) Cytotoxic effects of RuPOP@MSNs on various human cancer and normal cells after 72-h incubation. Values expressed are means ± SD of triplicates. c) Flow cytometric analysis of A375 cells exposed to RuPOP@MSNs for 24 h. d) DNA fragmentation and nuclear condensation induced by RuPOP@MSNs (24 h) as determined by TUNEL-DAPI co-staining assay.

2.5. Induction of Cancer Cell Apoptosis by RuPOP@MSNs

Apoptosis was the most crucial mechanism accounting for the anticancer action of RuPOP.[27] Therefore, flow cytometry was used to examine the effects of MSNs on the action mechanisms of RuPOP. The representative DNA histograms clearly reveal that treatments of A375 cells with RuPOP@MSNs led to dose-dependent increase of apoptotic cell death, as evidenced by the increase in sub-G1 cell population (Figure 6c). The induction of cell apoptosis by the nanoparticles was further confirmed by TUNEL-DAPI co-staining assay, which could detect apoptotic DNA fragmentation and nuclear condensation before morphological change. As shown in Figure 6d, after incubation with RuPOP@MSNs, A375 cells exhibited typical apoptotic features including DNA fragmentation, nuclear condensation and formation of apoptotic bodies. These results indicate that RuPOP@MSNs inhibit cancer cell growth mainly through induction of apoptosis.

2.6. Activation of Extrinsic (Death Receptor-Mediated) Apoptotic Pathway by RuPOP@MSNs

Caspases family proteases are essential for the initiation and execution of cell apoptosis.[43] Cleavage of specific caspases and activation of downstream signals are important cellular evens during apoptosis of diverse biological systems.[44] Caspase-3 has been regarded as a central regulator of cell apoptosis, while caspase-8 and -9 act as initiators of extrinsic death receptor-mediated and intrinsic mitochondria-mediated apoptotic pathways. Therefore, in this study, we examined the roles of caspase family proteases in the apoptosis initiated by RuPOP@MSNs. As shown in **Figure 7**, treatments of the cells with RuPOP@MSNs led to dose-dependent activation of caspase-3, -8, and -10, but not caspase-9, which subsequently triggered the proteolytic cleavage of PARP, a characteristic hallmark of apoptosis. Moreover, the quantitative examination of caspase activities showed that RuPOP@MSNs evoked dose-dependent activation of caspase-3 and -8, but not caspase-9, in A375 cells, indicating the involvement of extrinsic pathway in cell apoptosis. Moreover, the protein expression levels of Fas and TNFR-2, two death receptors required for activation of caspase-8/10, as well as their adapter protein FADD, were also up-regulated (Figure 7d). RuPOP@MSNs also induced the truncation of Bid that could relay the apoptotic signal from the cell membrane into the cytosol. These results suggest that death receptor-mediated apoptotic pathway play an major role in apoptosis induced by RuPOP@MSNs, which is different from the free RuPOP that induces mitochondria-mediated apoptosis in cancer cells.[27]

2.7. ROS Overproduction Activates p53, AKT, and MAPKs Pathways

ROS is a essential chemical signal that regulates the signaling network triggered by various anticancer agents, including

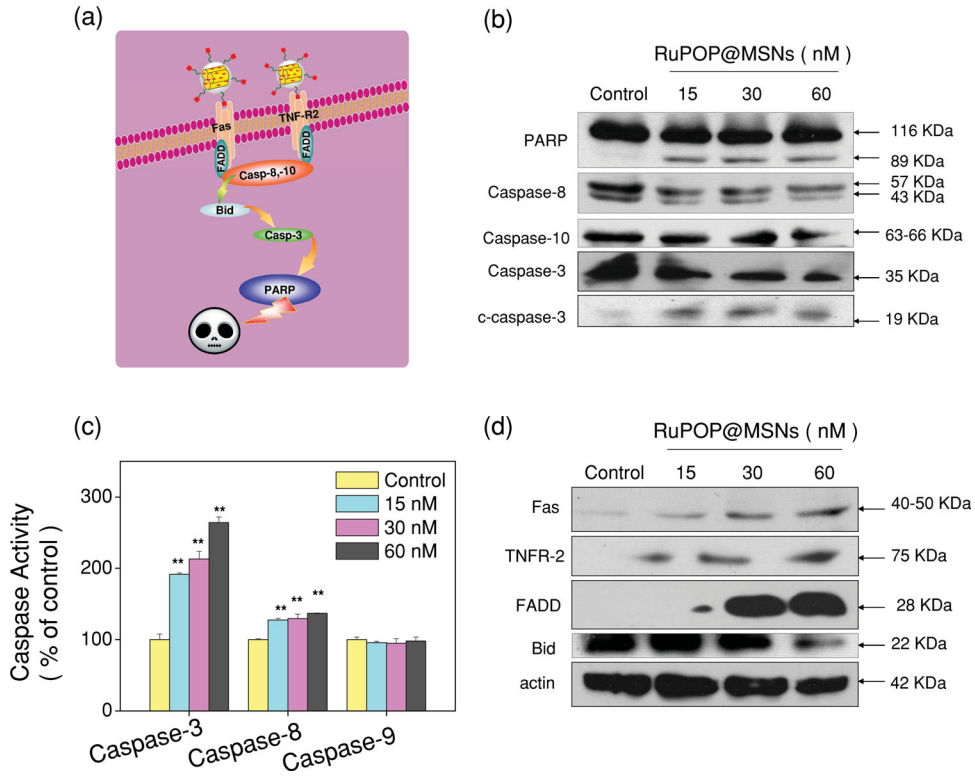

Figure 7. Activation of extrinsic apoptotic pathway by RuPOP@MSNs. a) Schematic illustration of death receptor-mediated apoptosis induced by RuPOP@MSNs in cancer cells. b) Activation of caspase family members in RuPOP@MSNs-induced apoptosis. c) Quantitative analysis of caspase activation triggered by RuPOP@MSNs. Cells were treated with RuPOP@MSNs for 24 h. Significant difference between treatment and control groups is indicated at $*P < 0.05$, $**P < 0.01$ level. d) Western blot analysis of expression levels of the death receptors after treated by RuPOP@MSNs. The data shown here are representative of four independent experiments with similar results.

cisplatin and Ru complexes.[28,45] A number of apoptotic stimuli induce cancer cell death through ROS overproduction.[46] Generally, excess ROS could attack various biological molecules, like proteins and DNA, leading to protein modification and DNA damage, which could trigger cell apoptosis through various downstream signaling pathways,[47] such as p53, ATM/ATR, AKT and MAPKs pathways.[48] Therefore, the ROS levels in cells exposed to RuPOP and RuPOP@MSNs was measured by DCF fluorescence method. As shown in **Figure 8**b, treatment of cells with RuPOP@MSNs led to a rapid increase in DCF fluorescence intensity in a time-dependent manner, which is much higher than that of 1.6 μM free RuPOP. To check the involvement of p53 pathway in cell apoptosis, we examined the expression levels of total and phosphorylated p53 in treated cells. As shown in Figure 8c, RuPOP@MSNs triggered the elevation of total p53 and its phosphorylation at Ser 15 site. The protein levels of p21Waf1, p-ATM, p-ATR, p-Chk2, p-BRCA1, and Ser139-Histone H2A.X (a DNA damage marker) were also increased in cells exposed to RuPOP@MSNs. Taken together, these results suggest that ROS-activated p53 phosphorylation is essential for apoptosis triggered by RuPOP@MSNs.

Due to the importance of MAPKs and AKT in the action of anticancer drugs, we examined the protein expression levels of total and phosphorylated MAPKs and AKT in cells treated with RuPOP@MSNs. As shown in Figure 8d, RuPOP@MSNs induced differential effects on p38, JNK, ERK, and AKT in cells exposed to RuPOP@MSNs. The phosphorylation of pro-apoptotic kinases p38 and JNK displayed a trend of up-regulation in a dose-dependent manner. In contrast, the phosphorylation of anti-apoptotic kinases ERK and AKT was effectively suppressed by RuPOP@MSNs. These results suggest that RuPOP@MSNs activate MAPKs and AKT pathways in cancer cells by regulating ROS generation. Following, we examined the effects of thiol-reducing antioxidants, N-acetylcysteine (NAC) and glutathione (GSH), on the cell death and ROS level, to confirm the importance of ROS in the anticancer action of RuPOP@MSNs. The results showed that NAC and GSH effectively inhibited the cell death (Figure 8e and Figure S8, Supporting Information) and ROS generation (Figure 8f) induced by RuPOP@MSNs, which confirm the importance of ROS to the apoptosis induced by RuPOP@MSNs.

3. Conclusions

In conclusion, we have described the design and synthesis of a cancer-targeted nanomaterials loaded with a novel Ru polypyridyl complex that endow the direct fluorescence monitoring of the cellular uptake and localization of anticancer agents in cancer cells. Specifically, the RGD peptide surface

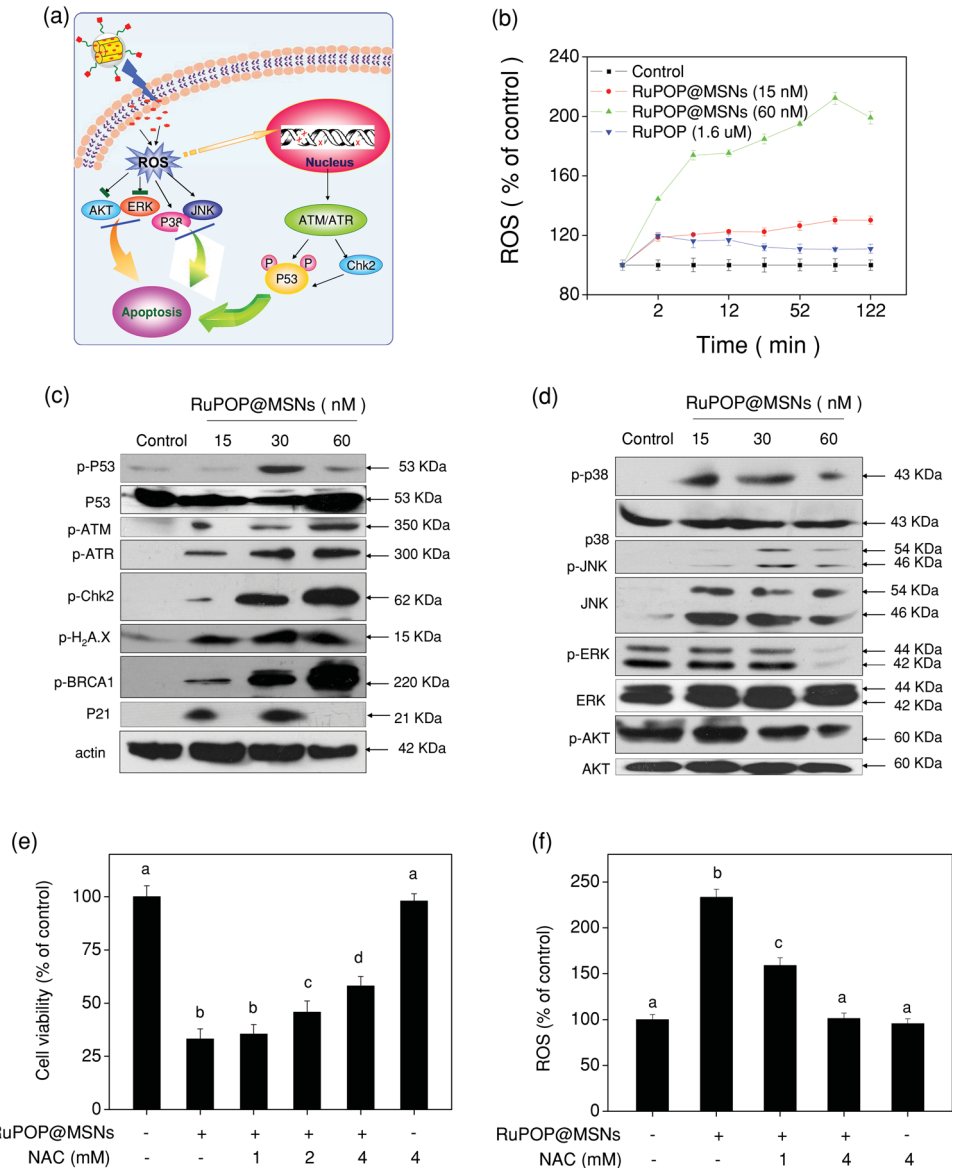

Figure 8. Activation of intracellular apoptotic signaling pathways by RuPOP@MSNs. a) Proposed apoptotic signaling pathways triggered by RuPOP@MSNs in A375 cells. b) Overproduction of ROS in A375 cells exposed to RuPOP@MSNs and RuPOP. c) Activation of p53 signaling pathway by RuPOP@MSNs. d) Effects of RuPOP@MSNs on the phosphorylation status and expression levels of MAPKs and AKT pathways. Cells were treated with different concentrations of RuPOP@MSNs for 24 h. e) Effects of NAC on cell growth inhibition induced by RuPOP@MSNs. Cells were pretreated with NAC for 2 h and then exposed to 0.1 μM RuPOP@MSNs for 24 h. Cell viability was determined by MTT assay. f) Effects of NAC on intracellular ROS generation induced by RuPOP@MSNs. Cells were pretreated with NAC for 2 h and then exposed to 0.1 μM RuPOP@MSNs for 1 h. All results were obtained from three independent experiments. Bars with different characters (a, b and c) are statistically different at $P < 0.05$ level.

decoration effectively enhances the cellular uptake of RuPOP@MSNs through receptor-mediated endocytosis, and improves the selectivity between cancer and normal cells. RuPOP@MSNs exhibits unprecedented enhanced cytotoxicity toward cancer cells overexpressing integrin receptor. The death receptor-mediated extrinsic pathway is essential for the apoptosis induced by RuPOP@MSNs. The internalized RuPOP@MSNs could release free Ru complex into the cytoplasm. The intracellular RuPOP triggers ROS overproduction, which could attack DNA in the nucleus and induce DNA damage-mediated p53 phosphorylation. In addition, ROS generation promotes cancer cell apoptosis through regulation of AKT and MAPKs signaling pathways. We anticipate that, this study may provide an effective strategy for the design and development of cancer-targeted agents that could achieve enhanced cellular uptake and anticancer efficacy.

4. Experimental Section

Synthesis of RuPOP@MSNs: The MSNs particles were synthesized according to previous procedures with modification.[6] Briefly, 2.0 g of the CTAC (Hexadecyl trimethyl ammonium chloride) were dissolved

in 20 mL water. Then added 50 µL of TEA (triethanolamine) into the mixed solution and then stirred 1 h at 95 °C. Then 1.5 mL of the TEOS (tetraethyl orthosilicate) was dropwise added in the mixed solution and then stirred for another 1 h. The products were collected by centrifugation and then refluxed in HCl/methanol for 6 h to remove the template CTAC. The MSNs was then collected by centrifugation and vacuum drying.

To obtain the MSNs-NH2 particles, 1.0 g of the MSNs particles was added to 50 mL of toluene. Then 1.0 mL of APTES ((3-aminopropyl) triethoxysilane) was dropwise added in the mixed solution and then refluxed for 24 h. The mixture was then extensively washed with toluene and ethanol and then vacuum drying. MSNs-SMP was then prepared by addition of 0.1 g of the MSNs-NH2 particles to the solution of the SMP with stirring for 24 h at room temperature. The obtained MSNs-SMP was added into 5 mL RGD solution and stirred 24 h. MSNs-RGD was then collected by centrifugation and vacuum drying. To obtain the RuPOP@MSNs particles, 50 mg of the MSNs-RGD particles was added to 5 mL of the RuPOP solution. The mixed solution was stirred for 48 h at room temperature, and then collected by centrifugation and vacuum drying. The concentration of RuPOP in the nanomaterials was determined by ICP-MS analysis.

Characterization of RuPOP@MSNs: The obtained product of the RuPOP@MSNs was characterized by transmission electron microscopy (TEM), scanning electron microscopy (SEM), Zetasizer particle size analysis, fourier transform infrared spectra (FT-IR), UV-visible spectroscopy, fluorescence spectroscopy and nitrogen adsorption-desorption technology. The samples for TEM analysis were prepared by dispersing RuPOP@MSNs onto the holey carbon film on copper grids. The micrographs were obtained on Hitachi H-7650 system with acceleration voltage set at 80 kV. SEM analysis was carried out on an EX-250 system (Horiba). FT-IR was recorded on a FT-IR spectrometer (Equinox 55, Bruker) in the range 4000–500 cm^{-1}. The Zeta potential and size distribution of the nanoparticles was analyzed on a Nano-ZS instrument (Malvern Instruments Limited). Nitrogen adsorption-desorption isotherms were obtained using a NOVA 4200e surface area analyzer (Quantachrome) at –196 °C under continuous adsorption conditions.

In Vitro Drug Release of RuPOP@MSNs: Briefly, 10 mg of RuPOP@MSNs powder was suspended in 10 mL of PBS at pH values of 7.4 and 5.3 with constant shaking at 37 °C in glass tube. After different incubation time, 0.5 mL of the supernatant was taken out from the glass tube and the same volume of fresh PBS was replaced. All samples were determined by fluorescence intensity with the excitation and emission wavelengths set at 479 and 599 nm, respectively.

Cell Culture and MTT Assay: Human cancer cell lines, including A375 melanoma cells, MCF-7 breast adenocarcinoma cells, HepG2 hepatocellular carcinoma cells, HepG2 drug resistance in hepatocellular carcinoma cells, and Neuro-2a mouse neuroblastoma cells, and HK-2 human proximal tubular cells were purchased from American Type Culture Collection (ATCC, Manassas, VA). The cells were cultured in DMEM media with 10% fetal bovine serum, 100 units mL^{-1} penicillin and 50 units/ml streptomycin at 37 °C in CO2 incubator (95% relative humidity, 5% CO2). Cell viability was determined by measuring by MTT assay.[49]

In Vitro Cellular Uptake of RuPOP@MSNs: Quantitative analysis of the cellular uptake of RuPOP@MSNs after different treatments was carried out as previously described.[50] Fluorescence microplate reader (SpectraMax M5, MD, USA) was used to measure the fluorescence intensity of RuPOP with excitation and emission wavelengths set at 479 and 599 nm, respectively. The cellular uptake efficiency was expressed as the percentage of nanoparticles adsorbed over that added.

Real-Time Live Cell Mornitoring: Real-time imaging of the cellular uptake and localization of RuPOP@MSNs was carried by living cell imaging technique under a monochromatic CoolSNAP FX camera (Roper Scientific, USA) and analysed by using AxioVision 4.2 software (Carl Zeiss).[50]

Flow Cytometric Analysis: The effects of RuPOP@MSNs on the cell cycle distribution were analyzed by flow cytometry as previously described.[51] Apoptotic cells with hypodiploid DNA content were measured by quantifying the sub-G1 peak in the cell cycle pattern.

TUNEL and DAPI Co-Staining Assay: DNA fragmentation and nucleus condensation induced by RuPOP@MSNs in cancer cells were examined by TUNEL-DAPI co-staining assay.[50]

Measurement of Intracellular Reactive Oxygen Species (ROS) Generation: The effects of RuPOP@MSNs on intracellular ROS generation in A375 cells were monitored by DCF-DA assay.[52] The intracellular ROS level was examined under a microplate reader (SpectraMax M5, MD) with the excitation and emission wavelengths at 479 and 599 nm, respectively.

Determination of Caspase Activity: Caspase activity was measured as previously described by using specific caspase-3, -8, -9 substrates.[52]

Western Blot Analysis: The effects of RuPOP@MSNs on the expression levels of proteins associated with different signaling pathways were examined by Western blot analysis.[52]

Statistics Analysis: All the data are expressed as mean ± standard deviation. Differences between the control and the experimental groups were analyzed by two-tailed Student's test. One-way analysis of variance (ANOVA) was used in multiple group comparisons. Statistical analysis was performed using SPSS statistical program version 13 (SPSS Inc., Chicago, IL). Difference with $P < 0.05$ (*) or $P < 0.01$ (**) was considered statistically significant.

Supporting Information

Supporting Information is available online from the Wiley Online Library or from the author. The surface area, pore volume and pore size of MSNs and RuPOP@MSNs (Table S1), size distribution of MSNs and RuPOP@MSNs (Figure S1), FT-IR spectra of the MSNs-RGD and RGD (Figure S2), conjugation of RGD peptide to MSNs as examined by BCA assay (Figure S3), comparison of the fluorescent spectra of RuPOP and RuPOP@MSNs (Figure S4), comparison of the cytotoxic effects of RuPOP@MSNs and RuPOP on various human cancer cells after treatments for 72 h (Figure S5), dose- and time-dependent growth inhibitory effects of RuPOP@MSNs on A375 and MCF-7 cells (Figure S6), effects of RGD-MSNs on the growth of various cancer and normal cells (Figure S7), and the effects of GSH on cell growth inhibition induced by RuPOP@MSNs (Figure S8).

Acknowledgements

This work was supported by National Science and Technology Support Program (2012BAC07B05), Science Foundation for Distinguished Young Scholars of Guangdong Province, Natural Science Foundation of China and Guangdong Province, Program for New Century Excellent Talents in University, Research Fund for the Doctoral Program of Higher Education of China and China Postdoctoral Science Foundation.

Received: October 15, 2013
Revised: November 21, 2013
Published online: January 27, 2014

[1] S. Nie, Y. Xing, G. J. Kim, J. W. Simons, *Annu. Rev. Biomed. Eng.* **2007**, *9*, 257.
[2] M. Shi, K. Ho, A. Keating, M. S. Shoichet, *Adv. Funct. Mater.* **2009**, *19*, 1689.
[3] P. Koley, A. Pramanik, *Adv. Funct. Mater.* **2011**, *21*, 4126.
[4] C. Minelli, S. B. Love, M. M. Stevens, *Small* **2010**, *6*, 2336.
[5] V. J. C. Y. Mohanraj, *Trop. J. Pharm. RES.* **2006**, *5*, 561.
[6] L. Pan, Q. He, J. Liu, Y. Chen, M. Ma, L. Zhang, J. Shi, *J. Am. Chem. Soc.* **2012**, *134*, 5722.

[7] M. Bruchez, Jr., M. Moronne, P. Gin, S. Weiss, A. P. Alivisatos, *Science* **1998**, *281*, 2013.
[8] A. G. Tkachenko, H. Xie, D. Coleman, W. Glomm, J. Ryan, M. F. Anderson, S. Franzen, D. L. Feldheim, *J. Am. Chem. Soc.* **2003**, *125*, 4700.
[9] D. Peer, J. M. Karp, S. Hong, O. C. FaroKHzad, R. Margalit, R. Langer, *Nat. Nanotechnol.* **2007**, *2*, 751.
[10] J. Shi, A. R. Votruba, O. C. Farokhzad, R. Langer, *Nano Lett.* **2010**, *10*, 3223.
[11] V. Lebret, L. Raehm, J. O. Durand, M. Smaihi, M. H. Werts, M. Blanchard-Desce, D. Methy-Gonnod, C. Dubernet, *J. Biomed. Nanotechnol.* **2010**, *6*, 176.
[12] S. Hudson, J. Cooney, E. Magner, *Angew. Chem. Int. Ed. Engl.* **2008**, *47*, 8582.
[13] J. L. Vivero-Escoto, I. I. Slowing, B. G. Trewyn, V. S. Lin, *Small* **2010**, *6*, 1952.
[14] M. Vallet-Regi, F. Balas, D. Arcos, *Angew. Chem. Int. Ed. Engl.* **2007**, *46*, 7548.
[15] E. Katz, I. Willner, *Angew. Chem. Int. Ed. Engl.* **2004**, *43*, 6042.
[16] R. Hao, R. Xing, Z. Xu, Y. Hou, S. Gao, S. Sun, *Adv. Mater.* **2010**, *22*, 2729.
[17] M. Liong, J. Lu, M. Kovochich, T. Xia, S. G. Ruehm, A. E. Nel, F. Tamanoi, J. I. Zink, *ACS Nano* **2008**, *2*, 889.
[18] J. M. Rosenholm, A. Meinander, E. Peuhu, R. Niemi, J. E. Eriksson, C. Sahlgren, M. Linden, *ACS Nano* **2009**, *3*, 197.
[19] J. M. Rosenholm, E. Peuhu, J. E. Eriksson, C. Sahlgren, M. Linden, *Nano Lett.* **2009**, *9*, 3308.
[20] N. Singh, A. Karambelkar, L. Gu, K. Lin, J. S. Miller, C. S. Chen, M. J. Sailor, S. N. Bhatia, *J. Am. Chem. Soc.* **2011**, *133*, 19582.
[21] C. Wang, Z. Li, D. Cao, Y. L. Zhao, J. W. Gaines, O. A. Bozdemir, M. W. Ambrogio, M. Frasconi, Y. Y. Botros, J. I. Zink, J. F. Stoddart, *Angew. Chem. Int. Ed. Engl.* **2012**, *51*, 5460.
[22] J. Lu, M. Liong, J. I. Zink, F. Tamanoi, *Small* **2007**, *3*, 1341.
[23] D. P. Ferris, J. Lu, C. Gothard, R. Yanes, C. R. Thomas, J. C. Olsen, J. F. Stoddart, F. Tamanoi, J. I. Zink, *Small* **2011**, *7*, 1816.
[24] Z. Tao, B. Toms, J. Goodisman, T. Asefa, *ACS Nano* **2010**, *4*, 789.
[25] M. Markman, *Expert Opin. Drug Saf.* **2003**, *2*, 597.
[26] P. C. Bruijnincx, P. J. Sadler, *Curr. Opin. Chem. Biol.* **2008**, *12*, 197.
[27] T. Chen, Y. Liu, W. J. Zheng, J. Liu, Y. S. Wong, *Inorg. Chem.* **2010**, *49*, 6366.
[28] L. Li, Y. S. Wong, T. Chen, C. Fan, W. Zheng, *Dalton Trans.* **2012**, *41*, 1138.
[29] X. Meng, M. L. Leyva, M. Jenny, I. Gross, S. Benosman, B. Fricker, S. Harlepp, P. Hebraud, A. Boos, P. Wlosik, P. Bischoff, C. Sirlin, M. Pfeffer, J. P. Loeffler, C. Gaiddon, *Cancer Res.* **2009**, *69*, 5458.
[30] V. Pierroz, T. Joshi, A. Leonidova, C. Mari, J. Schur, I. Ott, L. Spiccia, S. Ferrari, G. Gasser, *J. Am. Chem. Soc.* **2012**, *134*, 20376.
[31] K. K. Lo, A. W. Choi, W. H. Law, *Dalton Trans.* **2012**, *41*, 6021.
[32] M. R. Gill, J. A. Thomas, *Chem. Soc. Rev.* **2012**, *41*, 3179.
[33] C. A. Puckett, J. K. Barton, *J Am Chem Soc* **2009**, *131*, 8738.
[34] R. B. Elmes, K. N. Orange, S. M. Cloonan, D. C. Williams, T. Gunnlaugsson, *J. Am. Chem. Soc.* **2011**, *133*, 15862.
[35] E. Ozbay, *Science* **2006**, *311*, 189.
[36] U. H. Bunz, V. M. Rotello, *Angew. Chem. Int. Ed. Engl.* **2010**, *49*, 3268.
[37] A. T. Bell, *Science* **2003**, *299*, 1688.
[38] C. Kim, S. S. Agasti, Z. Zhu, L. Isaacs, V. M. Rotello, *Nat. Chem.* **2010**, *2*, 962.
[39] T. Inoue, P. G. Cavanaugh, P. A. Steck, N. Brunner, G. L. Nicolson, *J. Cell. Physiol.* **1993**, *156*, 212.
[40] H. N. Keer, J. M. Kozlowski, Y. C. Tsai, C. Lee, R. N. McEwan, J. T. Grayhack, *J. Urol.* **1990**, *143*, 381.
[41] E. Ryschich, G. Huszty, H. P. Knaebel, M. Hartel, M. W. Buchler, J. Schmidt, *Eur. J. Cancer* **2004**, *40*, 1418.
[42] F. Wang, Y. C. Wang, S. Dou, M. H. Xiong, T. M. Sun, J. Wang, *ACS Nano* **2011**, *5*, 3679.
[43] R. Sinha, K. Ei-Bayoumy, *Curr. Cancer Tar.* **2004**, *4*, 13.
[44] I. Budihardjo, H. Oliver, M. Lutter, X. Luo, X. Wang, *Annu. Rev. Cell Dev. Biol.* **1999**, *15*, 269.
[45] H. Pelicano, D. Carney, P. Huang, *Drug Resist. Update* **2004**, *7*, 97.
[46] K. Apel, H. Hirt, *Annu. Rev. Plant Bio.* **2004**, *55*, 373.
[47] D. R. Lloyd, D. H. Phillips, P. L. Carmichael, *Chem. Res. Toxicol.* **1997**, *10*, 393.
[48] T. Chen, Y. S. Wong, W. Zheng, Y. Bai, L. Huang, *Colloids Surf. B Biointerfaces* **2008**, *67*, 26.
[49] T. Chen, Y. S. Wong, *Biomed. Pharmacother.* **2009**, *63*, 105.
[50] W. Liu, X. L. Li, Y. S. Wong, W. J. Zheng, Y. B. Zhang, W. Q. Cao, T. F. Chen, *ACS Nano* **2012**, *6*, 6578.
[51] L. M. Wilhelmsson, F. Westerlund, P. Lincoln, B. Norden, *J. Am. Chem. Soc.* **2002**, *124*, 12092.
[52] T. Chen, Y. S. Wong, *Int. J. Biochem. Cell Biol.* **2009**, *41*, 666.